Soft-x-ray-induced ionization and fragmentation dynamics of $Sc_3N@C_{80}$ investigated using an ion-ion-coincidence momentum-imaging technique

Hui Xiong,[1] Razib Obaid,[1] Li Fang,[2] Cédric Bomme,[3] Nora G. Kling,[1] Utuq Ablikim,[4] Vladimir Petrovic,[5] Chelsea E. Liekhus-Schmaltz,[5] Heng Li,[5] Rene C. Bilodeau,[1] Thomas Wolf,[5] Timur Osipov,[6] Daniel Rolles,[4] and Nora Berrah[1]

[1]*Physics Department, University of Connecticut, Storrs, Connecticut 06269, USA*
[2]*Center for High Energy Density Science, University of Texas, Austin, Texas 78712, USA*
[3]*Deutsches Elektronen-Synchrotron (DESY), 22607 Hamburg, Germany*
[4]*James R. Macdonald Laboratory, Kansas State University, Manhattan, Kansas 66506, USA*
[5]*Stanford PULSE Institute, SLAC National Accelerator Laboratory, Menlo Park, California 94025, USA*
[6]*LCLS, National Accelerator Laboratory, Menlo Park, California 94025, USA*

(Received 3 July 2017; published 13 September 2017)

The fragmentation dynamics of an endohedral fullerene, $Sc_3N@C_{80}$, after absorption of a soft-x-ray photon, has been studied with an ion-ion-coincidence momentum-imaging technique. Molecular inner-shell ionization at 406.5 eV, targeting the Sc ($2p$) shell of the encapsulated Sc_3N moiety and the C ($1s$) shell of the C_{80} cage, leads to the cage fragmentation through evaporation of C_2, emission of small molecular carbon ions (C_n^+, $n \leqslant 24$), and release of Sc and Sc-containing ions associated with the carbon cage opening or fragmentation. The predominant charge states of Sc and Sc-containing ionic fragments are +1 despite an effective Sc valence of 2.4, indicating that charge transfer or redistribution plays an important role in the fragmentation of the encaged Sc_3N. Sequential emission of two out of the three Sc atoms of the encaged moiety, via Coulomb explosion in the form of Sc^+ or Sc-containing ions, is significant. We also find that the resonant excitation of the Sc ($2p$) shell electrons significantly increased the yield of the parent $Sc_3N@C_{80}$ and its fragment ions, partially attributed to the collision of the energetic Auger electrons from the Sc site with the carbon cage.

DOI: 10.1103/PhysRevA.96.033408

I. INTRODUCTION

Fullerenes and their derivatives, characterized by their hollow geometric structures and nanometer-size outer diameter, draw a great deal of interest due to their wide range of applications and "supramolecular" physical and chemical properties [1]. For example, trimetallic nitride template (TNT) endohedral metallofullerenes (EMFs), which consist of a trimetallic nitride moiety and a fullerene host, have attracted broad interest in many fields, including organic chemistry, materials chemistry, biomedical chemistry, biomedicine, and molecular device design [2–5]. Particularly, EMFs may be used as radiotherapy agents to treat tumors while significantly reducing the x-ray dose for patients. Functional groups can be attached to the endohedral fullerene shell to bind the molecules to a specific site, delivering toxic high-Z metal atoms enclosed inside [6,7]. Endohedral fullerenes have high stability, an inherent advantage for resisting biologically induced cage opening [8], thus protecting healthy tissues from the toxic metals. Monochromatic x rays can then be used to resonantly excite the high-Z atom, restricting the x-ray radiation damage to the cells that need to be treated, while leaving surrounding tissues largely unaffected.

To achieve a full understanding of the interaction of EMFs with x rays, their fundamental dynamics and processes must be explored, which is currently in its infancy. In this work, we study $Sc_3N@C_{80}$ with photon energies of 299 eV, slightly above the ionization of the C K edge (∼284 eV), and ∼406 eV, which is around the Sc L_2 ($2p_{1/2}$) edge at 406.5 eV. We investigate the fragmentation dynamics at discrete photon energies in this range, while investigating the detailed processes underlying the ionization and fragmentation of $Sc_3N@C_{80}$ at around the Sc L_2 edge.

To uncover the underlying fragmentation dynamics, a detailed measurement of the absorption cross section in the gas phase is needed. However, the only available measurement is for a micron-size $Sc_3N@C_{80}$ crystal [9]. We thus estimate, based on Ref. [9], the cross section of $Sc_3N@C_{80}$ on resonance for exciting a Sc L_2 ($2p_{1/2}$) electron to the lowest unoccupied orbitals (LUMOs) to be 73 Mb by adding the cross section for Sc atoms (31 Mb) and that for the C_{80} carbon cage (42 Mb) [9]. Meanwhile, the off-resonance cross sections of the Sc L_2 resonance at 395 and 410 eV are estimated to be 45 and 49 Mb, respectively. At these two photon energies, the cross sections for the Sc atoms are ∼1 and 8 Mb, respectively, while the cross sections for the C_{80} carbon cage are 44 and 41 Mb, respectively. N in the Sc_3N moiety contributes a relatively small amount to the total cross section [9]. Comparing the fragment yields for x rays with different photon energies around the Sc L_2 ($2p_{1/2}$) edge reveals the role that the Sc L_2 ($2p_{1/2}$) shell vacancy plays in the ionization and fragmentation dynamics of $Sc_3N@C_{80}$.

The fragmentation of gas-phase C_{60} has been studied using nanosecond lasers [10], femtosecond visible and near-infrared lasers [11], synchrotron x-ray sources [12,13], free-electron lasers [14], and in collisions with atoms and molecules [15,16], ions [17–19], and electrons [20,21]. Fragmentation processes which have been observed include the emission of neutral C_2 (evaporation), the emission of charged C_2^+ (fission), and Coulomb explosion where molecular and atomic carbon ions are emitted. The fragmentation of endohedral fullerenes has been observed in experiments with femtosecond near-infrared lasers, nanosecond visible lasers, synchrotron x-ray sources, and x-ray free-electron lasers [9,22–35]. However, the studies regarding the fragmentation dynamics in endohedral fullerenes have mainly focused on neutral carbon dimer emission induced

by single x-ray photons or single-pulse lasers [29,30,32,34], or the formation of new chemical bonds [23,24,33]. A few experiments observed the emission of the encaged atoms or molecules [22–24,29,33,35,36], but only the kinetic energy release (KER) of the encaged N atom from $N@C_{60}^+$ and $N@C_{70}^+$ has been measured [27,28]. While for spectroscopy experiments only simple ion spectra are recorded, coincidence techniques, i.e., mapping the coincident emissions of electron-electron, electron-ion, ion-ion, and many other possible combinations, provide the additional information necessary to identify physical and chemical processes [37–39].

In this work, three different fragmentation processes—evaporation of C_2, emission of small molecular carbon ions (C_n^+, $n \leqslant 24$), and release of Sc and Sc-containing ions associated with carbon cage opening or fragmentation of $Sc_3N@C_{80}$ after inner-shell vacancy created in the Sc L_2 ($2p_{1/2}$) shell or C K shell—have been identified. The coincidence between the kinetic energy (KE) of Sc^+ and other fragments is used to determine the origin of the peaks observed in the Sc^+ kinetic energy distribution (KED). With the KE coincidence of Sc ions, we found that fragmentation through sequential emission of two Sc ions is significant. Finally, we discuss the role of a Sc ($2p$) vacancy in the ionization and fragmentation of the parent molecule.

II. EXPERIMENTAL TECHNIQUE

The experiment was carried out at the Advanced Light Source (ALS) beamline 8.0.1 which delivers photons between 80 and 1250 eV, with a photon flux from 10^{11} up to 6×10^{15} photons/s, depending on the photon energy and its resolution [40]. The photon-energy calibration was done by measuring the yield of N^+ ions (from the N_2 background) and matching it to a scan of N^+ yield as a function of x-ray photon energy from previous work [41]. The measurements were performed using a double-velocity map imaging (VMI) spectrometer and coincidence-capable detectors. The current setup was upgraded from our previous experimental setup [42,43] by replacing a simple flight tube on the electron side with a VMI spectrometer for electrons and was identical to the setup described in Ref. [44]. Although the electron side of the spectrometer is capable of measuring the two-dimensional momenta of the electrons in the detector plane, we only use it as the trigger to start the data acquisition in the current experiment. This spectrometer is optimized for multi-ion coincidence using the ALS multibunch mode of operation. The VMI spectrometer axis was aligned horizontally, which is parallel to the polarization of the synchrotron soft x rays and perpendicular to the molecular beam. A static electric field applied across the interaction region served to extract electrons and ions from the interaction region. The extracted ions were guided through a set of electrodes and a 50-cm-long drift tube, and were detected by a multihit-capable time- and position-sensitive detector (RoentDek). The time of flight of the ions was measured with respect to the arrival time of the first detected electron, which typically arrived at the electron detector after a flight time of about 5 ns. The detector hit positions and the time of flight (TOF) of the ions were used to reconstruct their three-dimensional (3D) momenta and KE.

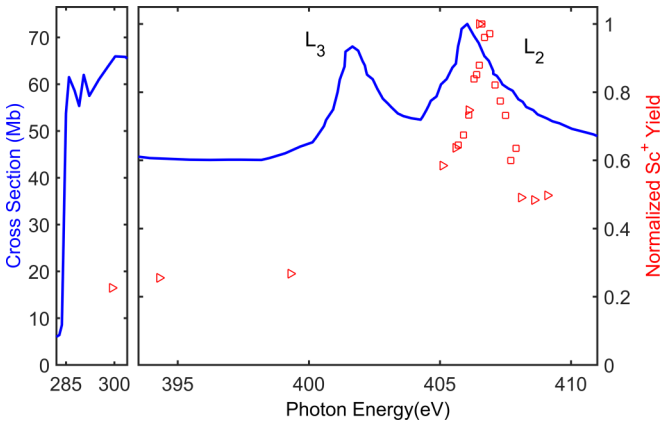

FIG. 1. Comparison between the measured Sc^+ ion yield from gas-phase $Sc_3N@C_{80}$ (red data points; squares and triangles depict two different data sets) and the absorption cross section of solid-phase $Sc_3N@C_{80}$ [9] (blue solid line) as functions of x-ray photon energy.

The $Sc_3N@C_{80}$ sample was obtained from SES Research and has a purity of 97%. Per the manufacturer, the primary impurity consists of C_{70}, along with some possible C_{76} and C_{78}. A gas-phase sample was obtained by evaporating $Sc_3N@C_{80}$ powder in an oven, heated to about 910 K. The evaporated molecules were introduced vertically into the interaction region through a nozzle and a 1-mm aperture. The pressure in the interaction chamber was $\sim 6 \times 10^{-9}$ Torr when the oven was set at the working temperature.

III. RESULTS AND DISCUSSION

A. Time-of-flight mass spectra

The photon energy for resonant excitation of the L_2 ($2p_{1/2}$) subshell electron of Sc to the lowest unoccupied molecular orbitals (LUMOs) of the endohedral fullerene is 406.5 eV, measured by scanning the Sc^+ ion yield. Figure 1 shows the yield of Sc^+ ions as a function of the incident x-ray photon energy in the range of the Sc ($2p$) absorption edge. We observe a strong resonance at 406.5 eV, which is assigned to the resonant excitation of an electron from the Sc L_2 ($2p_{1/2}$) subshell to the LUMO of the endohedral fullerene. The observed resonance energy is 0.8 eV blueshifted as compared to previous measurement of the absorption cross section of solid-phase $Sc_3N@C_{80}$ [9]. As for the Sc L_3 ($2p_{3/2}$) resonance peak, we were not able to extract it because it overlaps with the resonant excitation energy of the K-shell electron to the excited π^* states of N_2 from our background gas.

The spectra shown in Fig. 2 are taken at the 406.5 eV resonance. Since this photon energy is also above the C K edge, the probability of photoionization from the C ($1s$) electron is not negligible. Figure 2(a) shows the overall mass-to-charge (m/q) spectrum, in which the detector efficiency is not taken into account. At small m/q, i.e., less than 35 amu, the spectrum is dominated by H^+, C^+, N^+, O^+, and other ions (not shown here). We note that the C_2^+ yield is much smaller than H^+, C^+, N^+, O^+, and neutral fragments cannot be detected. Sc-containing molecular ion fragments, ScC_2^+, $ScCN^+$, ScC_3^+, and ScC_4^+, are observed, as well as atomic Sc^+ ions. The

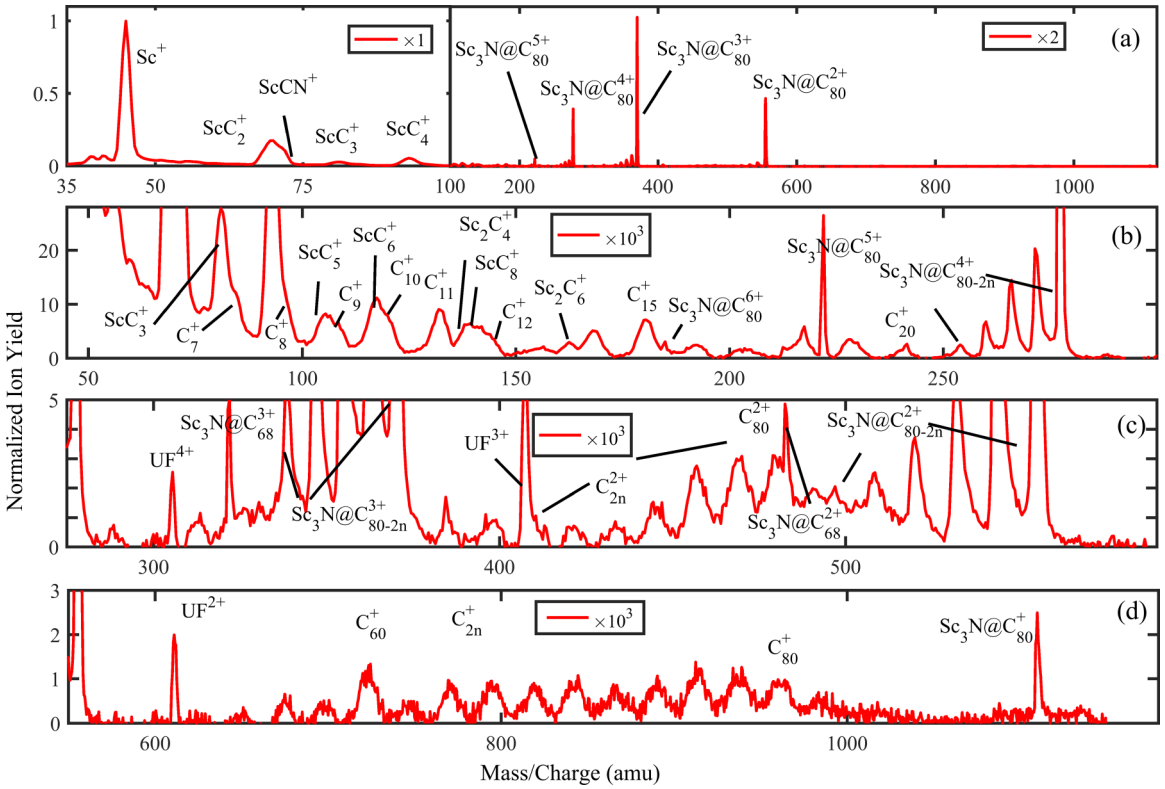

FIG. 2. Mass-to-charge (m/q) spectra, derived from the time-of-flight spectrum, of $Sc_3N@C_{80}$ acquired at a photon energy of 406.5 eV, i.e., the resonant excitation energy for excitation of Sc L_2 ($2p_{1/2}$) inner-shell electrons to the LUMO of the endohedral fullerene. (a) Overall m/q spectrum. The spectrum for $m/q > 100$ has been multiplied by 2. (b) Zoomed-in spectrum displaying molecular carbon and Sc-containing ions. In this panel, $0 \leqslant n \leqslant 4$ for $Sc_3N@C_{80-2n}{}^{4+}$. (c) Zoomed-in spectrum displaying peaks between the doubly and quadruply charged parent ions. In this panel, $0 \leqslant n \leqslant 4$ for $Sc_3N@C_{80-2n}{}^{2+}$ and $Sc_3N@C_{80-2n}{}^{3+}$, and $33 \leqslant n \leqslant 40$ for $C_{2n}{}^{2+}$. (d) Zoomed-in spectrum displaying peaks between singly and doubly charged parent ions. In this panel, $28 \leqslant n \leqslant 40$ for $C_{2n}{}^{+}$. The ion spectra in (b–d) are multiplied by 1000.

right side of Fig. 2(a) mainly consists of multiply charged parent molecules, up to the sextuply charged state, and the singly charged parent molecule is barely visible due to the low-absorption cross section of outer-shell electrons of C and Sc, while the absorption by C ($1s$) and Sc L_2 ($2p_{1/2}$) electrons creates an inner-shell vacancy, and leads to multiple charges on the parent molecule through cascade Auger processes. To identify low-yield ions, we zoomed in to the region between Sc^+ and $Sc_3N@C_{80}{}^{4+}$ shown in Fig. 2(b). In addition to those Sc carbides that contain only one Sc atom ($ScC_3{}^+$, $ScC_5{}^+$, $ScC_6{}^+$, and $ScC_8{}^+$), ions that contain two Sc atoms ($Sc_2C_4{}^+$ and $Sc_2C_6{}^+$) are observed. In Figs. 2(b) and 2(c), fullerene ions that have lost one or multiple C dimers from parent molecules, such as $Sc_3N@C_{78}{}^{4+}$, are found in doubly, triply, and quadruply charged states. Meanwhile, multiple peaks are also observed around the mass of pure molecular carbon C_{2n} ($28 \leqslant n \leqslant 40$), likely ionic fullerene fragments with cagelike structures [45], in singly and doubly charged states in Figs. 2(c) and 2(d). However, due to the isotopes of carbon and nitrogen, along with the peak broadening owing to recoil, we unfortunately were not able to distinguish fullerene ions, such as $C_{2n-1}N$, $Sc@C_{2n-4}$, and $ScNC_{2n-5}$, where $28 \leqslant n \leqslant 40$. In addition to fragments of $Sc_3N@C_{80}$, we observed a set of unknown fullerenes in doubly, triply, and quadruply charged states, with mass ~1222, marked as UF in Figs. 2(c) and 2(d). These peaks most likely originate from a small amount of this unknown fullerene contaminant when the sample was produced.

We can already identify a couple of fragmentation processes that also happen in the fragmentation of C_{60}, using the m/q spectra (see Fig. 2). The first process is the evaporation of one or multiple neutral C_2, a typical fragmentation process observed in C_{60} [11,46,47] and endohedral fullerenes [22–25] using IR lasers [24,46,47], and x rays from free-electron lasers [14,25]. The second process is fragmentation into many bodies, which creates small molecular carbon ions due to high excitation energy [25,48].

B. Ion-ion-coincidence results

Different from empty C_{60} or fullerene cage fragmentation in this work is the escape mechanism for the encapsulated Sc_3N moiety, which is unstable without the fullerene cage to stabilize it. As seen in Fig. 2, Sc^+ and Sc-containing ions are abundant fragments. While the generation of free metal ions as well as metal-containing molecular fragments from endohedral fullerenes has been experimentally observed using TOF spectroscopy [22–25,36], the underlying dynamics can be better understood with the additional information that is available from our ion-ion-coincidence experiment. Thus, in Fig. 3, we plot the KED of the Sc^+ fragments as a function of the m/q of the second fragment that was detected in

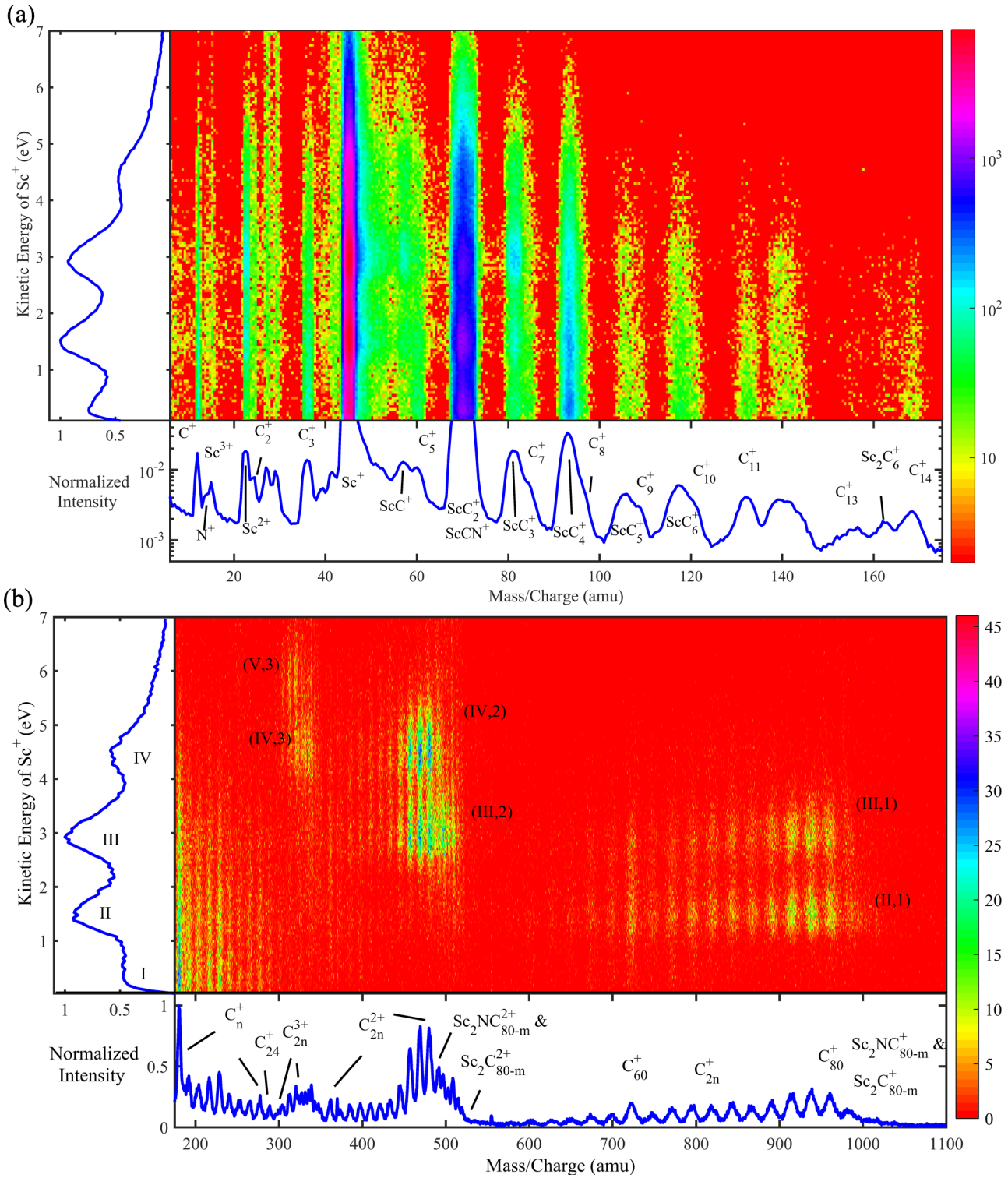

FIG. 3. Coincidence map of the Sc^+ KE and the mass-to-charge ratio of the ion detected in coincidence with Sc^+ at a photon energy of 406.5 eV (on resonance). Projections of the two-dimensional map are plotted in the bottom and left panels, representing the ion fragments coinciding with the Sc^+ ions and the KED of the Sc^+ ions, respectively. (a) $m/q < 175$; (b) $m/q > 175$; $15 \leqslant n \leqslant 24$ for $C_n{}^+$, $30 \leqslant n \leqslant 40$ for $C_{2n}{}^{2+}$, $38 \leqslant n \leqslant 40$ for $C_{2n}{}^{3+}$, and $25 \leqslant n \leqslant 40$ for $C_{2n}{}^+$; $0 \leqslant m \leqslant 7$ for $Sc_2NC_{80-m}{}^{2+}$ and $Sc_2NC_{80-m}{}^+$, $0 \leqslant m \leqslant 6$ for $Sc_2C_{80-m}{}^{2+}$ and $Sc_2C_{80-m}{}^+$.

coincidence with Sc^+. In Fig. 3(b), the four peaks of the Sc^+ KED are labeled from I to IV. On the coincidence map, a few islands appear, and indicate a coincidence between a Sc^+ (peaks II–IV) and a charged ionic fullerene fragment. Here, we mark the coincidence islands as (I–IV, 0–3), in which the first number denotes the Sc^+ KED peak and the second number denotes the charge state of the detected ionic fullerene fragment. We attribute the "quantized" behavior of the peaks

II–IV ions to the initial Coulomb repulsion between Sc^+ ions and corresponding residual ions with different charge states, which can then undergo further fragmentation.

Investigating the coincidence islands in Fig. 2, we find that the coincidence island (II, +1) corresponds to a Coulomb explosion that releases a peak II Sc^+ ion and a singly charged fullerene ion. Similarly, coincidence islands (III, +2) and (III, +1) correspond to Coulomb explosion fragmentation that releases peak III Sc^+ ions and is associated with the generation of doubly charged and singly charged fullerene ions correlated with Sc^+ ions, respectively. Since the peak III Sc^+ ion originates from intermediate or parent endohedral fullerenes with three charges, the coincidence island (III, +2) is consistent with the scenario that a triply charged parent or intermediate endohedral fullerene emits a Sc^+ ion, leaving a doubly charged fullerene. Then further relaxation by sequentially emitting a second Sc^+ ion leads to the coincidence island (III, +1). As for the peak IV Sc^+, two coincidence islands (IV, +3) and (IV, +2) were observed, but island (IV, +1) is absent. It is known that the parent fullerene is stabilized by the donation of multiple electrons from the encaged Sc_3N moiety to the cage [5]. In a neutral parent molecule, six electrons are donated from the encaged Sc_3N moiety to the cage to stabilize the molecule.

The Sc atoms have an effective charge of +2.4 in the neutral parent molecule [49]. After the creation of an inner-shell vacancy from the C or Sc atoms, cascade Auger electron processes lead to multiple-charge states of the parent molecules. Charge rearrangement leads to even higher charge states on those Sc atoms and may increase the Coulomb energy on the highly charged Sc_3N moiety. Emission of two Sc^+ or Sc-containing ions will significantly lower the tension inside the cage, while the only Sc left inside the cage may remain safely enclosed; thus this may explain why the coincidence island (IV, +1) is weak. The existence of the coincidence island (IV, +2) and (III, +1) indicates that emission of two encaged Sc atoms is possible.

Furthermore, several ionic fragments that would have been concealed using TOF spectroscopy alone due to overlapping with ions at similar m/q are identifiable in Fig. 3. In the projection of the mass spectrum, plotted in the bottom panel of Fig. 3(b), molecular carbon fragments up to C_{24}^+ are distinguishable, while the biggest molecular carbon fragment identified was only C_{20}^+ in Fig. 2(c). A series of fragments coinciding with peak III in the Sc^+ KED spectrum, namely, $Sc_2NC_{80-m}^{2+}$ ($0 \leqslant m \leqslant 7$) or/and $Sc_2C_{80-m}^{2+}$ ($0 \leqslant m \leqslant 6$), also emerge from the background.

To further examine the origin of the peaks in the KED of the Sc^+ ions, we plot the KEDs of Sc^+ ions coinciding with (a–c) ionic fullerene fragments at different charge states, (d) molecular carbon ions, (e) Sc^+, ScC_2^+, and $ScCN^+$ ions, (f) ions with $m/q < 40$ amu, and (g) all ions, as well as KED of (h) all Sc^+ ions in Fig. 4. Especially for the Sc^+ coinciding with high-m/q fragments, it is apparent that the different peaks of the KEDs of Sc^+ ions originate from parent or intermediate endohedral fullerenes with different charge states. For instance, peaks II and III of the KED of Sc^+ coincide with singly charged ionic fullerene fragments, while peaks III and IV coincide with doubly charged ionic fullerene fragments. For Sc^+ ions coinciding with $300 < m/q < 345$, we also

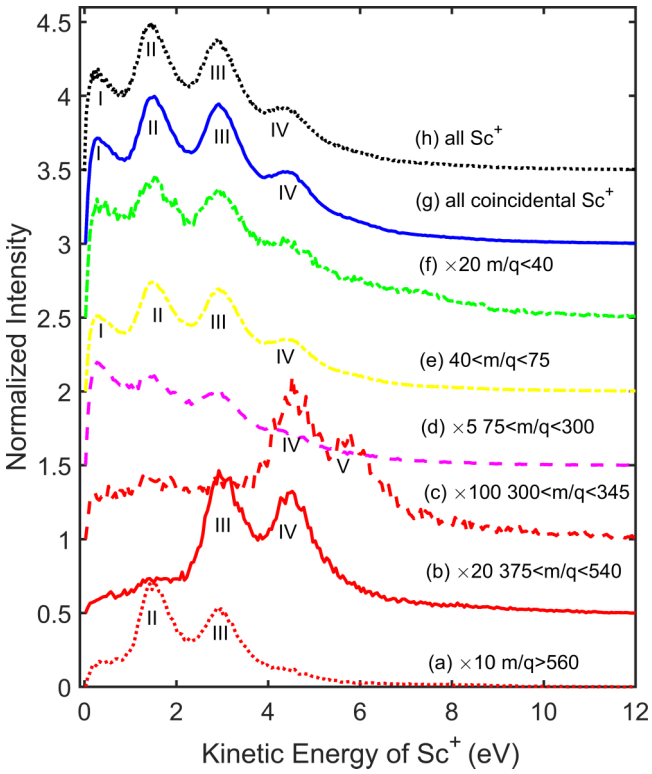

FIG. 4. KED of Sc^+ ions coinciding with (a) singly charged fullerene fragments at $m/q > 560$ amu; (b) doubly charged fullerene fragments at 200 amu $< m/q <$ 540 amu; (c) triply charged fullerene fragments at 300 amu $< m/q <$ 345 amu; (d) molecular carbon ions at 75 amu $< m/q <$ 300 amu; (e) mainly Sc^+, ScC_2^+, and $ScCN^+$ ions at 40 amu $< m/q <$ 75 amu; (f) $m/q <$ 40 amu (g) all ions. (a–g) are normalized with the maximum in (e). (h) Normalized KED of all Sc^+ ions.

notice the emergence of another peak at higher energy, labeled V, which we attribute to the Coulomb repulsion between a Sc^+ ion and a quadruply charged ionic fullerene residual ion. The four peaks in Fig. 4 are centered at 1.4, 2.9, 4.4, and 6.0 eV. These almost equally spaced peaks are consistent with the conclusion that they originate from an initial Coulomb repulsion process, where the fullerene cage opens such that a Sc^+ is released, as summarized in Table I. Interestingly, a KE of 1.4 eV corresponds to ~50% of the Coulomb energy when two charges are put at a distance of 0.5 nm, which is approximately the sum of the radii of the C_{80} cage (0.415 nm) and Sc^{2+} ion (0.11 nm) as defined in [50]. Consideration of the carbon cage as a conducting sphere can lower the expected KE of Sc^+ ions, but it cannot account for this 50% difference [51,52]. Similar energy loss was also observed in the fragmentation of multiply charged fullerene dimers into two charged monomers [51,53,54], where about half of the Coulomb energy was converted to internal energy of the fullerene monomers.

The KED of Sc^+ ions that coincide with small molecular carbon ions C_n^+ ($8 \leqslant m \leqslant 24$) are shown as (d) in Fig. 4, consisting of mostly a base and small contributions from peak I to V. To create small molecular carbon ions other than neutral C_2 dimer from the fragmentation of isolated (gas-phase) C_{60} and C_{60}^+, Campbell *et al.* established that an average internal energy of 100 eV is needed with a simple

TABLE I. Summary of the mechanisms producing selected Sc^+ ions with a photon energy of 406.5 eV. The originating charge refers to the charged on the parent or intermediate endohedral fullerene before the emission of a Sc^+, while the residual charge refers to the charge on the intermediate or final fullerene fragment after the emission of a Sc^+.

Peak	Originating charge	Residual charge	Mechanism	Energy (eV)	Proportion (%)
I	+1	0	Cage opening, escaping	0.36	7.9
II	+2	+1	Cage opening, Coulomb repulsion	1.4	11.5
III	+3	+2	Cage opening, Coulomb repulsion	2.9	14.7
IV	+4	+3	Cage opening, Coulomb repulsion	4.5	8.8
V	+5	+4	Cage opening, Coulomb repulsion	6.0	0.5
VI	Unknown		Cage multiple fragmentation, Coulomb explosion	3.0	56.7

statistical theory [55]. Thus we assume that high internal energy is also required to create small molecular carbon ions from $Sc_3N@C_{80}$, although it is complicated since the interaction between the internal Sc_3N moiety and the cage should also be considered. To dispose of the high internal energy, multiple fragmentation occurs [56]. According to previous theoretical and experimental studies, most molecular carbon ions containing less than 30 carbon ions are chain and ring structured [57–61]. Therefore, the base may originate from the following scenario: (1) The high internal energy leads to multiple fragmentation into small molecular carbon ions, and Sc is attached to one of the fragments; (2) the Sc-containing intermediate ion goes through further fragmentation, and releases a Sc^+ ion and molecular carbon ions.

We assume the close-to-zero peak I comes from a fragmentation process that releases a Sc^+ ion and a neutral fullerene. Peak I thus corresponds to an escaping mechanism which, without Coulomb repulsion, gives rise to a nearly zero KE. Similar phenomena have been observed in the "escape" of a neutral N atom from $N@C_{60}^+$ and $N@C_{70}^+$ [27,28], due to thermal instability. We note that for peak I in Fig. 4(g), the KED of Sc^+ ions coinciding with other ions are mostly contributed by Sc^+ ions coinciding with a second Sc^+ ion or Sc-containing ions, which is discussed later (see discussion on Fig. 6). The Sc^+ at peak I is rarely coincident with ionic fullerene fragments, while on the contrary, Sc^+ at peaks II–IV tend to appear with multiply charged fullerene fragments.

In order for the Sc^+ to be released from the carbon cage, the cage can either gently open or undergo a more violent Coulomb explosion. According to Ref. [62], the encapsulation binding energy (EBE) of $Sc_3N@C_{80}$ can be evaluated with the following equation,

$$E_{\mathrm{EBE}} = \Delta E_{\mathrm{DE}} + \Delta E_{\mathrm{ST}} + \Delta E_{\mathrm{ORB}}, \tag{1}$$

where the first term, ΔE_{DE}, is the deformation energy needed to convert the Sc_3N moiety and C_{80} from their equilibrium geometries to the overall molecule, $Sc_3N@C_{80}$. The second term, ΔE_{ST}, represents the repulsion between the Sc_3N^{6+} and C_{80}^{6-}, and the last term, ΔE_{ORB}, is the orbital interaction term due to the energy lowering upon electron donation from the Sc_3N moiety to the cage. Given that the calculated ΔE_{DE}, ΔE_{ST}, and ΔE_{ORB} are 1.37, 20.7, and −33.04 eV [62], the EBE for $Sc_3N@C_{80}$ is −11.60 eV, where the negative sign means that energy must be put into the system to remove the Sc_3N moiety from the cage. The EBE is approximately 2 eV higher than the activation energy of C_2 loss on ionic $Sc_3N@C_{80}$ [63], and does not include the energy needed for deforming the carbon cage to release the Sc_3N moiety. Therefore, the carbon bond cleavage without fragmentation, or simply "cage opening," is favored in the early stages of the release of Sc^+. During the cage opening, the Sc_3N moiety is also likely to be disturbed due to the delicate electronic balance between the encaged Sc_3N moiety and the cage. Part of the Sc_3N moiety may breach the cage through the broken bonds that have not regained their equilibrium. During the breach, charge is transferred or redistributed from the Sc ions to the rest of the fullerene, leading to predominantly +1 as the observed charge state of Sc and Sc-containing ions [25], despite the effective Sc valence of 2.4 in neutral $Sc_3N@C_{80}$ [49].

To further understand the dynamics that led to the production of Sc^+ ion, we examine its KED shown as the black dot line in Fig. 5(a). The red solid line is the sum of base fits corresponding to different assumed mechanisms. The fitting results are also summarized in Table I. To fit the KED, the tail is determined by the "model-free" method by Klots [64], as has been used intensively in other work [27,30,51,65–68],

$$P(\epsilon) = a\epsilon^{l}\exp\left(-l\frac{\epsilon}{\tilde{\epsilon}}\right), \tag{2}$$

where a is a normalization factor, $\tilde{\epsilon}$ is the position of the maximum of the distribution (i.e., the most probable KE value), and l is a parameter related to the interaction potential between the fragments ($0 < l < 1$). The tail fit is shown as the blue dash-dot-dot line in Fig. 5(a), labeled as VI. For the best fitting, l is found to be close to 1, which means that the KED is a "four-dimensional distribution that corresponds to a reaction with a large centrifugal barrier" [68]. The parameter l was found to be $\sim\frac{1}{2}$ in measurements of the kinetic energy release distributions (KERDs), which characterizes the total KE of all fragments, for the emission of (1) a neutral carbon dimer

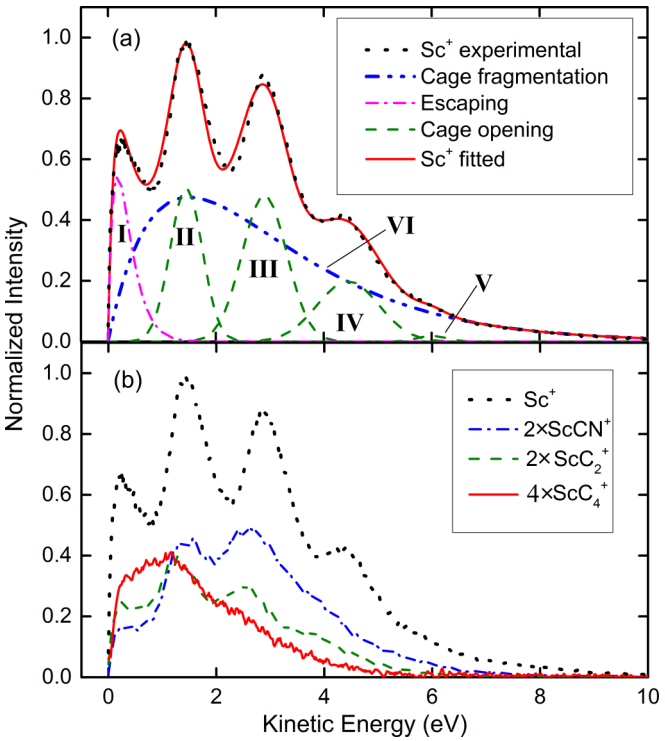

FIG. 5. KEDs of Sc^+ and Sc-containing ions for a photon energy of 406.5 eV. (a) KED of Sc^+ ionic fragments. The black dot and red solid lines are the experimental results and the sum of the KE spectrum fits, respectively. The fitted spectrum consists of components corresponding to ions generated by different mechanisms, as described in the text, shown in blue dash-dot-dot, pink dash-dot, and dashed green lines, respectively. (b) KEDs of Sc^+, ScC_2^+, $ScCN^+$, and ScC_4^+ ions.

C_2 from C_{60}^+, C_{70}^+, $Ti_2@C_{80}^+$, and $Sc_3N@C_{80}^+$ [69]; (2) C_2^+ from multiply charged C_{60} or C_{70} [52]; and (3) N from $N@C_{60}^+$ and $N@C_{70}^+$ [27,28]. Multiple fragmentation of the parent molecule can lead to broadened KED peaks, and may explain peak VI [similar to our interpretation of Fig. 4(d)].

The peak close to zero KE is also fitted with the model-free method, and is labeled as I. The parameter l for this peak was found to be close to 1 as well. As we discussed before, this peak originates from an escape mechanism that releases a Sc^+ ion from a singly charged parent or intermediate endohedral fullerene. The next four almost equally spaced peaks are fit with Gaussian functions. Since the whole fragmentation process is complex, this fitting procedure is somewhat of an oversimplification, and the fitting is rather qualitative. We do observe some discrepancy from the fitting to the experimental result, mainly caused by the selection of symmetric Gaussian distributions for fitting peaks II–V.

Interestingly, sometimes an escaping Sc atom will bring part of the fullerene cage with it. We examine the KEDs of three Sc-containing fragments, ScC_2^+, $ScCN^+$, and ScC_4^+, in Fig. 5(b). To reconstruct the KEDs of the ScC_2^+ and $ScCN^+$ ions, we selected the cleanly measured half of the distribution and multiplied the yield by 2 to compensate for the excluded ions. The final KEDs of ScC_2^+, $ScCN^+$, and ScC_4^+ ions were then scaled by a factor of 2, 2, and 4, respectively, for better visibility. The KEDs of these three fragments represent similar features compared to the contributions of Sc^+ from escaping, and Coulomb explosion mechanisms.

To understand the relation between the fragmentation mechanisms, we extract the KE coincidence between Sc^+ and Sc^+ ions and between Sc^+ and $ScCN^+$ ions, as shown in Fig. 6. The coincidences between the KE of two Sc^+ ions

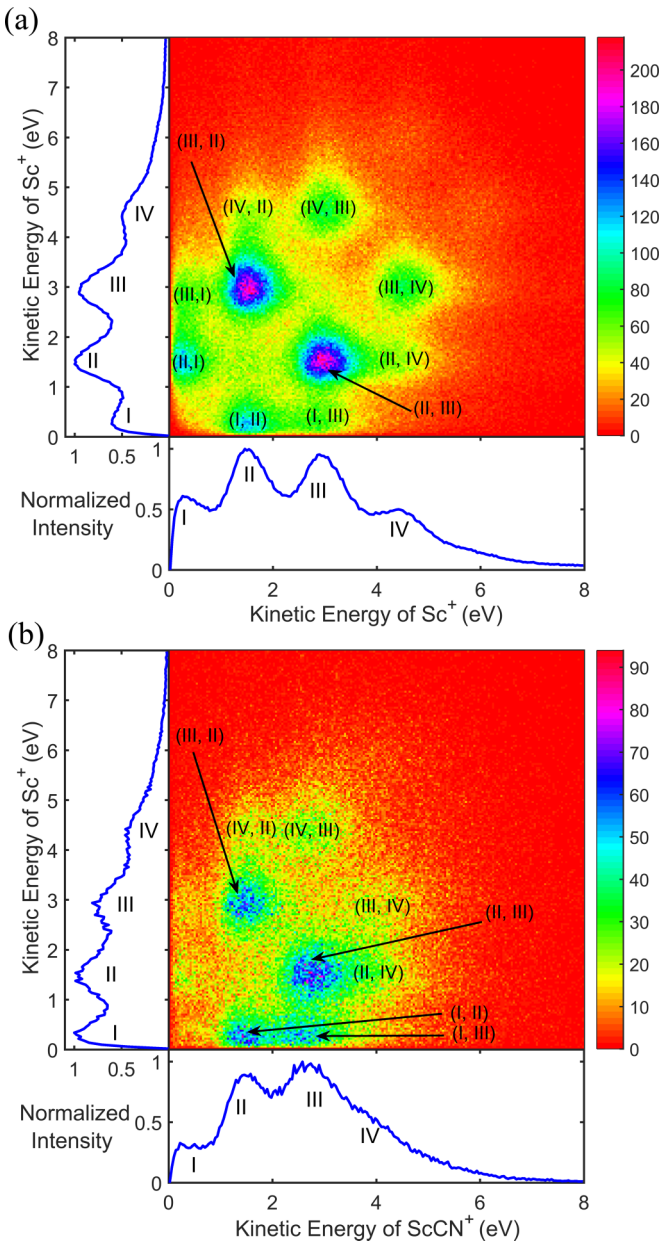

FIG. 6. (a) Coincidence map of the KE of two coinciding Sc^+ ions with a photon energy of 406.5 eV (on resonance). Projections of the two-dimensional map are plotted at the bottom and left panels, representing the KED of coinciding Sc^+ ions. Here the labels, such as (III, II), represent coincidence of two Sc^+ ions by Coulomb repulsion and cage opening fragmentation mechanism III and II individually. (b) Same as (a), but of coinciding Sc^+ and $ScCN^+$ ions; here the first and second Roman numerals indicate the origin of Sc^+ and $ScCN^+$ ions, respectively. Projections of the two-dimensional map are plotted in the bottom and left panels, representing the KED of coinciding $ScCN^+$ and Sc^+ ions.

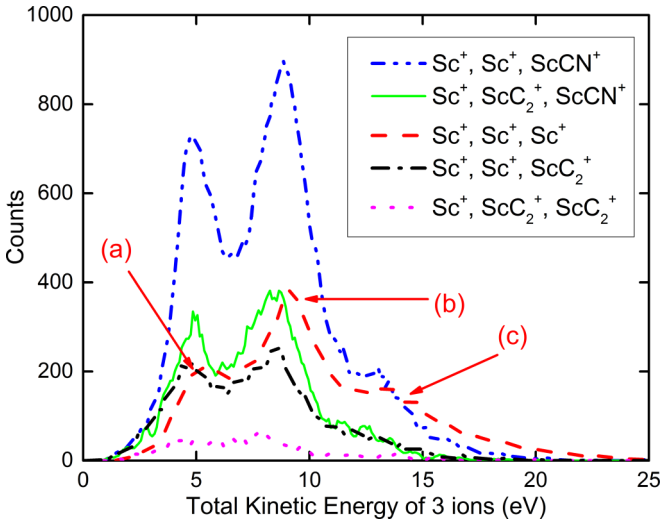

FIG. 7. Total KE of all three coinciding Sc^+ or Sc-containing ions following interaction with 406.5-eV photons (on resonance). Three arrows (a)–(c) mark the center of the three peaks for three coinciding Sc^+ ions.

are shown in Fig. 6(a). Roman numerals (I–IV) represent the fragmentation mechanisms (see details in Table I) for the Sc^+ fragments. A few prominent coincidence islands can be seen in Fig. 6(a). These islands can be classified in two sets. One set of islands is made up of those with two Roman numerals that differ by 1, such as (II, I), (I, II), (III, II), (II, III), (IV, III), (III, IV). For example, the coincidence island (II, I) represents a correlation of one Sc^+ from mechanism II and the other Sc^+ originates from mechanism I. As can be seen in Table I, during the fragmentation processes, the parent molecules experience at least two charge states, +2 and +1, which emit Sc^+ ions sequentially, to appear on this island. Therefore, the sequential emission of Sc^+ ions is a significant channel for the emission of more than one Sc^+ fragment. The other set of islands is made up of those with two Roman numerals that differ by 2, such as (IV, II), (II, IV), (III, I), and (I, III). To appear on these islands, the parent molecule must experience three charge states. Similar correlation maps are also found in the coincidence KE of (Sc^+, $ScCN^+$) and (Sc^+, ScC_2^+) (not shown here). In comparison with the KE coincidence between Sc^+ and Sc^+ ions, the (III, I) and (II, I) channels for coincidence between Sc^+ and $ScCN^+$ ions are weak, which indicates that there is a preference in emission order, since channels (I, III) and (I, II) are still prominent. It is worth mentioning that peak I contributes significantly (7.9%) to the total Sc^+ yield (see Table I), which is likely due to the emission of Sc^+ from a singly charged intermediate endohedral fullerene (i.e., an ionic fragment may have already been lost prior to the release of the Sc^+).

Despite the experimental challenge to measure three ions in coincidence, we also observed triple coincidence channels, where all Sc atoms are accounted for, and the sum of their KEs is shown in Fig. 7. Interestingly, the strongest channel is for coincidence among 2-Sc^+ and 1-$ScCN^+$. In general, the total KE plot exhibits three peaks. Again, we interpret the peaks as sequential emission of the Sc^+ ions from a triply [peak (a)], quadruply [peak (b)], and quintuply [peak (c)] charged parent or intermediate molecule. For instance, peak (b) originates from the 4+ parent or intermediate molecule charge state. Emission of three Sc^+ ions may follow three sequential Coulomb explosions (IV, III, and II), which are the first, second, and third fragmentation processes releasing a Sc^+ ion. The average KEs for Sc^+ ions from the corresponding Coulomb repulsions are 4.5, 2.9, and 1.4 eV, per Table I. The sum of these three KEs is 8.8 eV, close to the position of peak (b) at 9.2 eV. We found that the positions of the three peaks (a, b, c) are very close to the experimental result, as summarized in Table II.

C. Photon-energy dependence of the fragmentation process

To clarify the role of a vacancy on the Sc L_2 shell in the ionization and fragmentation of the fullerene, we compare, in Fig. 8, the yields of Sc^+ and Sc-containing ionic fragments (ScC_2^+, $ScCN^+$, and ScC_4^+), $Sc_3N@C_{80-2n}^{2+}$ ($n = 1, 2$), $Sc_3N@C_{80-2n}^{3+}$ ($n = 1, 2, 3$), C_{2n}^+ ($35 \leqslant n \leqslant 40$), and the parent molecular ion yield, up to a quintuply charged state acquired at four different photon energies. The lowest photon energy of 299.3 eV is just above the C K edge and thus ionization of the C atoms forming the cage dominates. The other photon energies are below the Sc L edge (394.3 eV), on the Sc L_2 resonance (406.5 eV), and above the Sc resonance (409.1 eV).

The yield of the singly charged parent molecule, $Sc_3N@C_{80}^+$, is strongest for the 299.3-eV photon energy. This is likely due to the recapture of a slow photoelectron from a C ($1s$) orbital on the cage, similar to the observation made in C_{60} x-ray photon absorption [12,70]. For the other charge states ($n = 2, 3, 4, 5$) of the parent molecule shown in Fig. 8(b), the yields are all maximum at the Sc L_2 resonance at 406.5 eV, as expected.

It was suggested by Ref. [49] that the emission of a neutral carbon dimer requires more than 40-eV internal energy from C_{60}. Thus fragmentation processes that emit neutral carbon dimers depend not only on the charge states, but also on some excess internal energy. The yield ratios (R) of $Sc_3N@C_{80}^{2+}$ to

TABLE II. We list the three peak positions of the total energy of three coinciding Sc^+ ions shown in Fig. 7 (with photon at 406.5 eV on resonance). The nth ($n = 1-3$) in the table refers to the nth fragmentation process that emits a Sc^+ ion. The KE of each fragmentation process is taken from Table I.

Peak	Peak energy (eV)	Parent charge state	First process, KE (eV)	Second process, KE (eV)	Third process, KE (eV)	Sum KE of Sc^+ in three processes (eV)	Offset (eV)
(a)	5.3	+3	III, 2.9	II, 1.4	I, 0.36	4.7	0.6
(b)	9.2	+4	IV, 4.5	III, 2.9	II, 1.4	8.8	0.4
(c)	13.4	+5	V, 6.0	IV, 4.5	III, 2.9	13.4	0

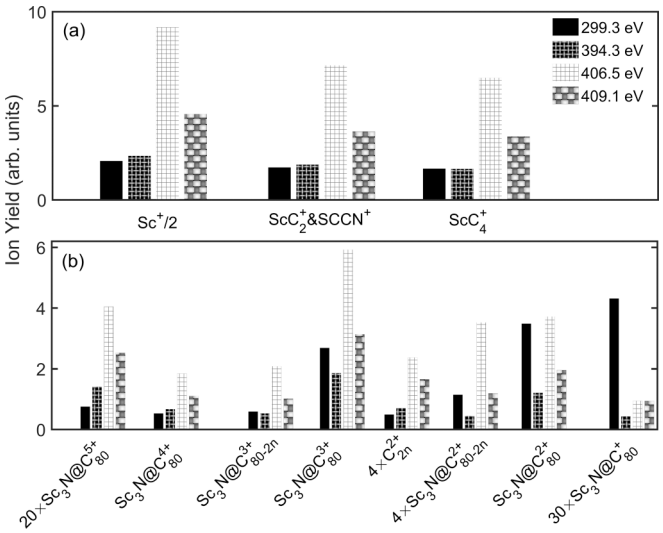

FIG. 8. Comparison of selected ion yields acquired at photon energies of 299.3, 394.3, 406.5 eV (on resonance), and 409.1 eV. Panel (a) shows the Sc and Sc-containing fragment ions while panel (b) shows the parent molecular ions up to quintuply charged, and $C_{2n}{}^{+}$ ($35 \leqslant n \leqslant 40$), $Sc_3N@C_{80-2n}{}^{2+}$ ($n = 1, 2$), $Sc_3N@C_{80-2n}{}^{3+}$ ($n = 1, 2, 3$).

$Sc_3N@C_{80-2n}{}^{2+}$ at photon energy 299.3 eV ($R = 12.2 \pm 1.0$) and 394.3 eV ($R = 10.9 \pm 1.6$) are much higher than that at 406.5 eV ($R = 4.2 \pm 0.4$) and 409.1 eV ($R = 6.5 \pm 0.4$). From the observed ion yield ratio between $Sc_3N@C_{80-2n}{}^{2+}$ and $Sc_3N@C_{80}{}^{2+}$, the order of the internal energies inside $Sc_3N@C_{80}{}^{2+}$ with respect to the x-ray photon energies is (on the Sc L_2 resonance, 406.5 eV) > (above the Sc L_2 edge, 409.1 eV) > (below the Sc $2p$ edge, 399.3eV) ≈ (just above the C K edge, 299.3 eV). We observe a similar trend with the ratio of $Sc_3N@C_{80-2n}{}^{3+}$ yield to that of $Sc_3N@C_{80}{}^{3+}$. The yields of Sc^+ and Sc-containing ion fragments ($ScC_2{}^+$, $ScCN^+$, and $ScC_4{}^+$) with photon energies of 299.3, 394.3 eV are similar, as shown in Fig. 8(b). The yield at the photon energy above the Sc L_2 edge is double that at a photon energy of 394.3 eV, while it quadrupled for the Sc L_2 resonant photon energy. The dominant parent molecular ions were found in the +2, +3, and +4 charge states. These charge states are also the dominant charge states that emit Sc^+ and Sc-containing ion fragments. However, the yield ratios of the multiply charged parent molecules between the photon energy of 406.5 and 399.3 eV are all around 3, lower than the observed yield ratio of 4 for Sc^+ and Sc-containing ion fragments. As we mentioned before, the release of Sc^+ requires energy to cleave carbon bonds; thus higher internal energy benefits the yield of Sc^+ ions. If a vacancy is created on the Sc ($2p$) shell, LMM Auger processes may emit energetic electrons around 300 eV, and even higher if the valence states are involved [71]. It was reported that the collision of a 200-eV electron on $Er_3N@C_{80}$ can result in quadruply charged parent molecules and lead to fragmentation by the emission of neutral carbon dimers, or Er^+ [18]. Since the Auger electrons emitted from the Sc sites are inside the cage, the chance of collision between the Auger electron and the carbon cage is high, leading to higher average internal energy than that if a C ($2s$) vacancy is generated on the carbon cage. Therefore, vacancy generated on a Sc ($2p$) shell leads to a higher yield of Sc^+ and Sc-containing ions. Furthermore, it is known that evaporation of neutral C_2 and generation of small molecular carbon ions also relies on the internal energy to enable cleavage of multiple carbon bonds. Therefore, the yields of a neutral carbon dimer, Sc or Sc-containing ions, and ionic carbon molecules from $Sc_3N@C_{80}$ subsequent to vacancy generated at the inner shell *all* depend on the internal energy accumulated during the relaxation processes.

Based on previous knowledge of C_{60} relaxation [72,73] studied with femtosecond lasers, electron-electron coupling and electron-photon coupling play important roles in redistributing the absorbed energy from the strong femtosecond laser field. Thus our data support the following internal energy accumulation scenario: Upon absorption of an x-ray photon by either the carbon K shell or the Sc L shell, relaxation through the electrons takes place immediately. First, in general, the extra energy is likely to be relaxed through Auger decay, and cascade Auger processes lead to a multiply charged parent molecule. Second, electron-electron coupling, with a typical time scale of around 50 fs [72], redistributes the charges and relaxes the energy into the electronic system of both the encaged Sc_3N moiety and the carbon cage. Third, electron phonon coupling, occurring on a time scale of around a few hundredths of a femtosecond [74], ensues and redistributes the energy between the electronic system and the nuclear backbone. Since there are hundreds of electrons on the carbon cage, electron-electron and electron-phonon coupling may be very efficient for thermalizing the parent molecule. Hence the fragmentation occurs due to the further relaxation of the thermalized molecule as well as the Coulomb energy [75] introduced by multiple charges resulting from cascade Auger processes.

IV. CONCLUSION

We investigated the inner-shell ionization and the subsequent fragmentation of $Sc_3N@C_{80}$ with a multicoincidence technique which permitted a detailed view of the fragmentation mechanisms. Three different fragmentation processes, (1) evaporation of C_2, (2) emission of small molecular carbon ions ($C_n{}^+$, $n \leqslant 24$), and (3) release of Sc and Sc-containing ions associated with carbon cage opening or fragmentation, are the most significant processes following core-shell ionization of Sc L_2 and C ($1s$). With the ion-ion-coincidence technique, we found that the sequential release of two ions, Sc^+ or Sc-containing ions, is significant, while the sequential emission of all three encaged Sc is less likely, but also possible. The excitation of a Sc L_2 electron on resonance increases the yield of the charged parent molecule and the ionic fragments from $Sc_3N@C_{80}$. The energetic electron (generated from the Sc site from inside the cage) colliding with the cage may account for the yield increase. We deduce that the internal energy of $Sc_3N@C_{80}$, which may be deposited during the relaxation process by electron-electron and electron-phonon coupling, plays an important role in all the fragmentation mechanisms.

ACKNOWLEDGMENTS

This work was funded by the Department of Energy, Office of Science, Basic Energy Sciences (BES),

Division of Chemical Sciences, Geosciences, and Biosciences under Grants No. DE-SC0012376 (U Conn group) and No. DE-FG02-86ER13491 (Kansas group). We gratefully acknowledge Wolfgang Eberhardt reading this manuscript and giving us helpful comments. L.F. acknowledges the support by Defense Advanced Research Project Agency Contract No. 12-63-PULSE-FP014, and by National Nuclear Security Administration Cooperative Agreement No. DE-NA0002008. C.B. was supported by the Helmholtz Gemeinschaft through the Helmholtz Young Investigator Program. We thank the staff of the Advanced Light Source for their support before and during the experiment; in particular we thank Wanli Yang and David Kilcoyne for their support.

[1] N. Martin and J.-F. Nierengarten, *Supramolecular Chemistry of Fullerenes and Carbon Nanotubes* (Wiley-VCH Verlag, Berlin, 2012).
[2] P. P. Fatouros, F. D. Corwin, Z.-J. Chen, W. C. Broaddus, J. L. Tatum, B. Kettenmann, Z. Ge, H. W. Gibson, J. L. Russ, A. P. Leonard *et al.*, Radiology **240**, 756 (2006).
[3] H. L. Fillmore, M. D. Shultz, S. C. Henderson, P. Cooper, W. C. Broaddus, Z. J. Chen, C.-Y. Shu, J. Zhang, J. Ge, H. C. Dorn *et al.*, Nanomedicine **6**, 449 (2011).
[4] A. A. Popov, S. Yang, and L. Dunsch, Chem. Rev. **113**, 5989 (2013).
[5] J. Zhang, S. Stevenson, and H. C. Dorn, Acc. Chem. Res. **46**, 1548 (2013).
[6] D. W. Cagle, S. J. Kennel, S. Mirzadeh, J. M. Alford, and L. J. Wilson, Proc. Natl. Acad. Sci. USA **96**, 5182 (1999).
[7] J. Meng, X. Liang, X. Chen, and Y. Zhao, Integr. Biol. **5**, 43 (2013).
[8] S. Stevenson, G. Rice, T. Glass, K. Harich, F. Cromer, M. R. Jordan, J. Craft, E. Hadju, R. Bible, M. M. Olmstead *et al.*, Nature **401**, 55 (1999).
[9] A. Müller, S. Schippers, R. A. Phaneuf, M. Habibi, D. Esteves, J. C. Wang, A. L. D. Kilcoyne, A. Aguilar, S. Yang, and L. Dunsch, J. Phys.: Conf. Ser. **88**, 012038 (2007).
[10] C. Lifshitz, Int. J. Mass Spectrom. **200**, 423 (2000).
[11] I. V. Hertel, T. Laarmann, and C. P. Schulz, Adv. At., Mol. Opt. Phys. **50**, 219 (2005).
[12] S. Aksela, E. Nõmmiste, J. Jauhiainen, E. Kukk, J. Karvonen, H. G. Berry, S. L. Sorensen, and H. Aksela, Phys. Rev. Lett. **75**, 2112 (1995).
[13] A. Reinköster, S. Korica, G. Prümper, J. Viefhaus, K. Godehusen, O. Schwarzkopf, M. Mast, and A. Becker, J. Phys. B **37**, 2135 (2004).
[14] B. F. Murphy, T. Osipov, Z. Jurek, L. Fang, S.-K. Son, M. Mucke, J. H. D. Eland, V. Zhaunerchyk, R. Feifel, L. Avaldi *et al.*, Nat. Commun. **5**, 4281 (2014).
[15] M. C. Larsen, P. Hvelplund, M. O. Larsson, and H. Shen, Eur. Phys. J. D **5**, 283 (1999).
[16] P. Hvelplund, L. H. Andersen, H. K. Haugen, J. Lindhard, D. C. Lorents, R. Malhotra, and R. Ruoff, Phys. Rev. Lett. **69**, 1915 (1992).
[17] J. Jensen, H. Zettergren, H. T. Schmidt, H. Cederquist, S. Tomita, S. B. Nielsen, J. Rangama, P. Hvelplund, B. Manil, and B. A. Huber, Phys. Rev. A **69**, 053203 (2004).
[18] B. Walch, C. L. Cocke, R. Voelpel, and E. Salzborn, Phys. Rev. Lett. **72**, 1439 (1994).
[19] H. Cederquist, A. Fardi, K. Haghighat, A. Langereis, H. T. Schmidt, S. H. Schwartz, J. C. Levin, I. A. Sellin, H. Lebius, B. Huber, M. O. Larsson, and P. Hvelplund, Phys. Rev. A **61**, 022712 (2000).
[20] M. S. Baba, T. S. L. Narasimhan, R. Balasubramanian, and C. K. Mathews, J. Phys. Chem. **99**, 3020 (1995).
[21] P. Scheier, B. Dünser, R. Wörgötter, D. Muigg, S. Matt, O. Echt, M. Foltin, and T. D. Märk, Phys. Rev. Lett. **77**, 2654 (1996).
[22] A. Stibor, H. Schefzyk, and J. Fortagh, Phys. Chem. Chem. Phys. **12**, 13076 (2010).
[23] A. Lassesson, A. Gromov, K. Mehlig, A. Taninaka, H. Shinohara, and E. E. B. Campbell, J. Chem. Phys. **119**, 5591 (2003).
[24] A. Lassesson, K. Hansen, M. Jönsson, A. Gromov, E. E. B. Campbell, M. Boyle, D. Pop, C. P. Schulz, I. V. Hertel, A. Taninaka *et al.*, Eur. Phys. J. D **34**, 205 (2005).
[25] N. Berrah, B. Murphy, H. Xiong, L. Fang, T. Osipov, E. Kukk, M. Guehr, R. Feifel, V. S. Petrovic, K. R. Ferguson *et al.*, J. Mod. Opt. **63**, 390 (2016).
[26] J. Hellhund, A. Borovik, K. Holste, S. Klumpp, M. Martins, S. Ricz, S. Schippers, and A. Müller, Phys. Rev. A **92**, 013413 (2015).
[27] B. Cao, T. Peres, C. Lifshitz, R. J. Cross, and M. Saunders, Chem. Eur. J. **12**, 2213 (2006).
[28] B. Cao, T. Peres, R. J. Cross, M. Saunders, and C. Lifshitz, J. Phys. Chem. A **105**, 2142 (2001).
[29] D. C. Lorents, D. H. Yu, C. Brink, N. Jensen, and P. Hvelplund, Chem. Phys. Lett. **236**, 141 (1995).
[30] J. Laskin, H. A. Jimenez-Vazquez, R. Shimshi, M. Saunders, M. S. de Vries, and C. Lifshitz, Chem. Phys. Lett. **242**, 249 (1995).
[31] A. L. D. Kilcoyne, A. Aguilar, A. Müller, S. Schippers, C. Cisneros, G. Alna'Washi, N. B. Aryal, K. K. Baral, D. A. Esteves, C. M. Thomas, and R. A. Phaneuf, Phys. Rev. Lett. **105**, 213001 (2010).
[32] J. Laskin, T. Peres, A. Khong, H. A. Jiménez-Vázquez, R. J. Cross, M. Saunders, D. S. Bethune, M. S. de Vries, and C. Lifshitz, Int. J. Mass Spectrom. **185–187**, 61 (1999).
[33] S. Suzuki, Y. Kojima, H. Shiromaru, Y. Achiba, T. Wakabayashi, R. Tellgmann, E. E. B. Campbell, and I. V. Herte, Z. Phys. D **40**, 410 (1997).
[34] A. Lassesson, K. Mehlig, A. Gromov, A. Taninaka, H. Shinohara, and E. E. Campbell, J. Chem. Phys. **117**, 9811 (2002).
[35] F. Rohmund, A. V. Bulgakov, M. Hedén, A. Lassesson, and E. E. B. Campbell, Chem. Phys. Lett. **323**, 173 (2000).
[36] H. Xiong, B. Mignolet, L. Fang, T. Osipov, T. J. A. Wolf, E. Sistrunk, M. Gühr, F. Remacle, and N. Berrah, Sci. Rep. **7**, 121 (2017).
[37] M. J. Van Stipdonk, E. A. Schweikert, and M. A. Park, J. Mass Spectrom. **32**, 1151 (1997).
[38] M. Sabbar, S. Heuser, R. Boge, M. Lucchini, L. Gallmann, C. Cirelli, and U. Keller, Rev. Sci. Instrum. **85**, 103113 (2014).
[39] T. Arion and U. Hergenhahn, J. Electron. Spectrosc. Relat. Phenom. **200**, 222 (2015).

[40] https://www.als.lbl.gov/beamlines/8-0-1/.
[41] E. Shigemasa, T. Gejo, M. Nagasono, T. Hatsui, and N. Kosugi, Phys. Rev. A **66**, 022508 (2002).
[42] Z. D. Pešic, D. Rolles, M. Perri, R. C. Bilodeau, G. D. Ackerman, B. S. Rude, A. L. D. Kilcoyne, J. D. Bozek, and N. Berrah, J. Electron. Spectrosc. Relat. Phenom. **155**, 155 (2007).
[43] Z. D. Pešić, D. Rolles, I. Dumitriu, and N. Berrah, Phys. Rev. A **82**, 013401 (2010).
[44] U. Ablikim, C. Bomme, H. Xiong, E. Savelyev, R. Obaid, B. Kaderiya, S. Augustin, K. Schnorr, I. Dumitriu, T. Osipov *et al.*, Sci. Rep. **6**, 38202 (2016).
[45] Q.-W. Yu and Y.-Q. Feng, in *Handbook of Nanophysics* (CRC Press, Boca Raton, FL, 2010), p. 1.
[46] M. H. K. Tchaplyguine, O. Dühr, H. Hohmann, G. Korn, H. W. M. H. I. V. Rottke, and E. E. B. Campbell, J. Chem. Phys. **112**, 2781 (2000).
[47] E. E. Campbell, K. Hansen, M. Heden, M. Kjellberg, and A. V. Bulgakov, Photochem. Photobiol. Sci. **5**, 1183 (2006).
[48] S. Cheng, H. G. Berry, R. W. Dunford, H. Esbensen, D. S. Gemmell, E. P. Kanter, T. LeBrun, and W. Bauer, Phys. Rev. A **54**, 3182 (1996).
[49] L. Alvarez, T. Pichler, P. Georgi, T. Schwieger, H. Peisert, L. Dunsch, Z. Hu, M. Knupfer, J. Fink, P. Bressler, M. Mast, and M. S. Golden, Phys. Rev. B **66**, 035107 (2002).
[50] A. V. Korol and A. V. Solov'yov, J. Phys. B **44**, 085001 (2011).
[51] B. Manil, L. Maunoury, J. Jensen, H. Cederquist, H. T. Schmidt, H. Zettergren, P. Hvelplund, S. Tomita, and B. A. Huber, Nucl. Instrum. Methods Phys. Res., Sect. B **235**, 419 (2005).
[52] N. Haag, Z. Berényi, P. Reinhed, D. Fischer, M. Gudmundsson, H. A. B. Johansson, H. T. Schmidt, H. Cederquist, and H. Zettergren, Phys. Rev. A **78**, 043201 (2008).
[53] H. Zettergren, H. T. Schmidt, P. Reinhed, H. Cederquist, J. Jensen, P. Hvelplund, S. Tomita, B. Manil, J. Rangama, and B. A. Huber, Phys. Rev. A **75**, 051201(R) (2007).
[54] H. Zettergren, H. T. Schmidt, P. Reinhed, H. Cederquist, J. Jensen, P. Hvelplund, S. Tomita, B. Manil, J. Rangama, and B. A. Huber, J. Chem. Phys. **126**, 224303 (2007).
[55] E. E. B. Campbell, T. Raz, and R. D. Levine, Chem. Phys. Lett. **253**, 261 (1996).
[56] R. Ehlich, M. Westerburg, and E. E. Campbell, J. Chem. Phys. **104**, 1900 (1996).
[57] G. von Helden, M. T. Hsu, P. R. Kemper, and M. T. Bowers, J. Chem. Phys. **95**, 3835 (1991).
[58] J. Hunter, J. Fye, and M. F. Jarrold, J. Chem. Phys. **99**, 1785 (1993).
[59] J. Hunter, J. Fye, and M. F. Jarrold, J. Phys. Chem. **97**, 3460 (1993).
[60] G. von Helden, N. G. Gotts, and M. T. Bowers, J. Am. Chem. Soc. **115**, 4363 (1993).
[61] G. von Helden, N. G. Gotts, and M. T. Bowers, Nature **363**, 60 (1993).
[62] J. M. C. Campanera Alsina, Ph.D. thesis, Rovira i Virgili University, 2004.
[63] K. Gluch, S. Feil, S. Matt-Leubner, O. Echt, P. Scheier, and T. D. Märk, J. Phys. Chem. A **108**, 6990 (2004).
[64] C. E. Klots, Z. Phys. D **21**, 335 (1991).
[65] M.-A. Lebeault, B. Baguenard, B. Concina, F. Calvo, B. Climen, F. Lépine, and C. Bordas, J. Chem. Phys. **137**, 054312 (2012).
[66] K. Gluch, S. Matt-Leubner, O. Echt, R. Deng, J. U. Andersen, P. Scheier, and T. D. Märk, Chem. Phys. Lett. **385**, 449 (2004).
[67] S. Matt, O. Echt, M. Sonderegger, R. David, P. Scheier, J. Laskin, C. Lifshitz, and T. D. Märk, Chem. Phys. Lett. **303**, 379 (1999).
[68] J. Laskin and C. Lifshitz, J. Mass Spectrom. **36**, 459 (2001).
[69] T. Peres, B. Cao, H. Shinohara, and C. Lifshitz, Int. J. Mass Spectrom. **228**, 181 (2003).
[70] S. Korica, Ph.D. thesis, Technischen Universität Berlin, 2006.
[71] D. K. G. de Boer, C. Haas, and G. A. Sawatzky, J. Phys. F **14**, 2769 (1984).
[72] I. Shchatsinin, T. Laarmann, G. Stibenz, G. Steinmeyer, A. Stalmashonak, N. Zhavoronkov, C. P. Schulz, and I. V. Hertel, J. Chem. Phys. **125**, 194320 (2006).
[73] I. Shchatsinin, T. Laarmann, N. Zhavoronkov, C. P. Schulz, and I. V. Hertel, J. Chem. Phys. **129**, 204308 (2008).
[74] J. R. Verlet, Chem. Soc. Rev. **37**, 505 (2008).
[75] S. Díaz-Tendero, M. Alcamí, and F. Martín, Phys. Rev. Lett. **95**, 013401 (2005).